Robust Charge Transfer Plasmons in Metallic Particle-Film Systems

Bijesh Kafle,^{†,‡,§} Paul Gieri,^{¶,§} Hamed Kookhaee,^{†,‡} Tefera E. Tesema,^{†,‡} Sharmin Haq,^{¶,‡} Alejandro Manjavacas,*,[¶] and Terefe G. Habteyes*,^{†,‡}

†Department of Chemistry and Chemical Biology, University of New Mexico, Albuquerque,
New Mexico 87131, United States

‡Center for High Technology Materials, University of New Mexico, Albuquerque, New Mexico 87131, United States

¶Department of Physics and Astronomy, University of New Mexico, Albuquerque, New Mexico 87131, United States

 $\S Authors\ contributed\ equally\ to\ this\ paper$

E-mail: manjavacas@unm.edu; habteyes@unm.edu

Abstract

Understanding how the plasmonic response of a metallic nanoparticle is modified by its coupling with a metallic film is a fundamental research problem relevant for many applications including sensing, solar energy harvesting, spectroscopy, and photochemistry. Despite significant research effort on this topic, the nature of the interaction between colloidal nanoparticles and metallic films is not fully understood. Here, we investigate, both experimentally and theoretically, the optical response of surface ligand-coated gold nanorods interacting with gold films. We find that the scattering cross section of these systems is dominated by a charge transfer plasmon mode, for which charge flows between the particle and the film. The properties of this mode are dictated by the

characteristics of the particle-film junction, which makes the frequency of this charge transfer plasmon far less sensitive to the nanoparticle size and geometry than a typical dipolar plasmon mode excited in similar nanorods placed directly on a purely dielectric substrate. The results of this work serve to advance our understanding of the interaction between metallic nanoparticles and metallic films, as well as provide a method for creating more robust plasmonic platforms that are less affected by changes in the size of individual nanoparticles.

Keywords

Colloidal Nanoparticle, Metallic Film, Plasmons, Dark-Field, Substrate, Charge Transfer Plasmon

When illuminated, metallic nanostructures are capable of sustaining collective excitations of their conduction electrons, commonly known as surface plasmons. These excitations couple strongly to light, resulting in large cross sections, and producing significantly enhanced electric fields around the nanostructure.^{2,3} Thanks to these extraordinary properties, metallic nanostructures are being used to improve solar energy harvesting devices, 4 drive chemical reactions using light, 5-7 and increase the sensitivity of biosensors, 8-11 to cite some relevant applications. The characteristics of a plasmon resonance are determined by the shape, size, and material properties of the metallic nanostructure that supports it, as well as by the dielectric environment in which the nanostructure is located. ¹² A paradigmatic example of such dependence is the redshift experienced by the plasmon resonance of a metallic nanostructure when placed near a dielectric substrate. ¹³ The changes of the plasmonic response of the nanostructure become particularly strong if the substrate is metallic, due to the coupling with the conduction electrons of the latter, 14-18 which results in an extraordinary electric field concentrated in the gap separating the two systems. 19-23 This field enhancement is particularly large when molecular spacers on the nanometer scale are used. 24 Due to this effect, coupled metallic particle-film structures have been the subject of extensive research in recent years^{24–30} as a promising platform for achieving ultrasensitive molecule detection, ^{31–33} single molecule optomechanics, ³⁴ strong coupling, ³⁵ enhanced emission, ^{36–38} and color printing. ³⁹

Despite the significant research effort and widespread applications of particle-film plasmonic systems, the interaction between a colloidal nanoparticle and metal film is not fully understood. Chemically synthesized metal nanoparticles are inherently coated with surface ligands (organic molecules) that provide a natural spacer of a thickness on the order of a few nanometers. 40–44 The properties of this layer determine the nature of the interaction, and hence the plasmonic response of the coupled system. In particular, the existence of a conductive junction between the particle and the film enables a distinct type of plasmonic resonances, commonly referred to as charge transfer plasmons, 45 in which the charge oscillates between the two systems. 46 These modes have been extensively investigated in particle dimers due to their potential for sensing applications, 45,47–49 as well as for being a robust platform to observe quantum plasmonic effects. 50–53

Here, we investigate how the optical response of colloidal metallic nanoparticles is modified as a result of the interaction with metallic substrates. To that end, we analyze the scattering spectra of individual gold nanorods of different sizes deposited both on silica and gold substrates. We find that, when they are placed on the metallic substrate, the scattering response of the nanorods is dominated by a charge transfer plasmon mode, in which charges oscillate between the substrate and the nanorod. Surprisingly, the resonance frequency of this mode is only weakly dependent on the size and width of the nanorods, which is in sharp contrast with the behavior shown by nanorods with similar sizes when they are placed on the purely dielectric substrate, in which case the scattering spectrum is dominated by a dipolar mode whose spectral position varies strongly with the length and width of the nanorod. Using a combination of rigorous solutions of Maxwell's equations and a simple analytical model, we show that the properties of the charge transfer mode are solely determined by the local characteristics of the particle-film junction, and therefore are weakly sensitive to the dimensions of the particle. These results contribute to advancement of the

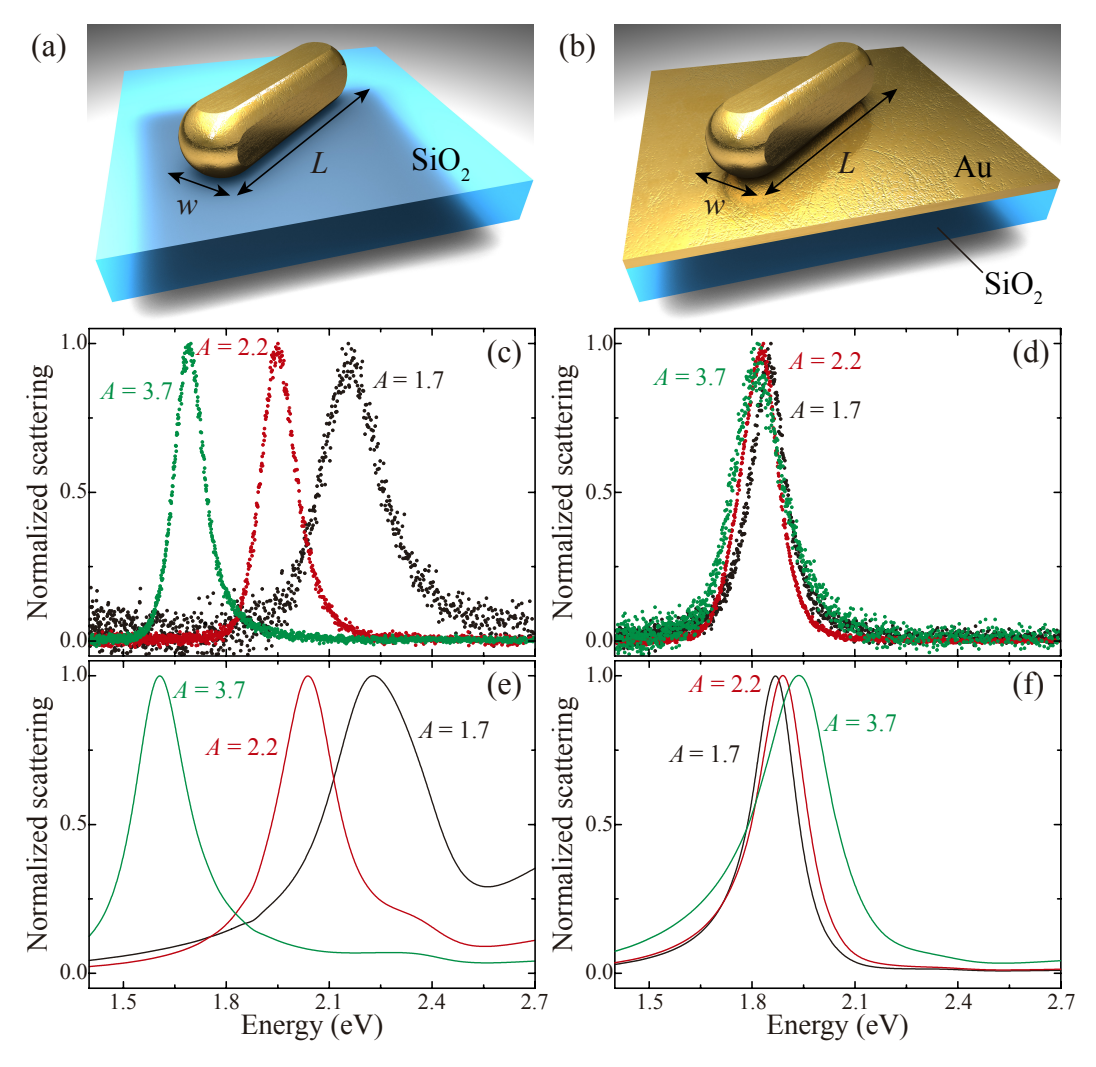


Figure 1: Optical response of gold nanorods placed on different substrates. (a,b) Schematics of the system under study consisting of a gold nanorod of length L and width w, placed directly on a silica substrate (a), or on a 50 nm-thick gold film deposited on silica (b). (c,d) Experimental single-particle scattering spectra for nanorods of width $w=40\,\mathrm{nm}$ and different aspect ratios A=L/w, as indicated by the labels, placed either on the silica (c) or gold (d) substrates. (e,f) Numerical simulations of the scattering spectrum of the nanorods of panels (c) and (d) performed by using a finite element method (FEM) approach. In all cases, the scattering spectra are normalized to their maximum value.

fundamental understanding of nanoparticle-film interactions, as well as to provide a basis for the development of plasmonic systems that are robust against differences in nanoparticle size.

The system under study is depicted in Figures 1(a) and (b). It consists of chemically synthesized gold nanorods of width w and length L, which are placed either directly on a silica substrate, or on a 50 nm-thick gold film deposited on silica (see the Supporting Information for details of the sample preparation). The nanorods are excited by focusing a ring of white light using dark-field objective of numerical aperture of 0.9 (see Figure S1 in the Supporting Information for more details on the experimental setup).

The normalized spectra measured for gold nanorods placed on the silica and gold substrates are shown in panels (c) and (d) of Figure 1, respectively. In each case, we analyze the scattering spectra of three different nanorods, all of them with the same width $w = 40 \,\mathrm{nm}$, but different aspect ratios A = L/w, as indicated by the labels in the plot. When deposited on the silica substrate, the scattering spectra of the gold nanorods display a single peak in the analyzed spectral region, whose location significantly depends on the aspect ratio of the nanorods, shifting to lower energies as the length of the rod increases. This is exactly the expected behavior for the longitudinal dipolar plasmon of the nanorod, whose energy is inversely proportional to the nanorod length. ¹² Interestingly, when nominally the same nanorods are, instead, placed on the gold film, we find that their corresponding scattering spectra converge to essentially the same resonance energy near 1.8 eV, regardless of the aspect ratio of the nanorods.

For the purpose of understanding this behavior, we calculate the scattering spectra for nanorods of the same dimensions by rigorously solving Maxwell's equations using a finite element method (FEM) approach. To reproduce the single crystalline nature of the nanorods, we model them as being faceted on four sides, with a facet width $w_f = 0.875w$ (see FigureS2 in the Supporting Information for a detailed description of our simulation geometry). In all cases, the nanorods are assumed to be in conductive contact with the substrate at one of

their facets. The choice of this configuration is based on the assumption that the surface ligands, which are initially coating the nanorods in solution, spread across the surface of the substrate during the deposition of the nanorods, which, together with the roughness of the substrate, enable a direct contact between them and the substrate. The validity of this assumption is confirmed later in the manuscript through experimental and theoretical evidences. The results of these calculations are shown in panels (e) and (f) of Figure 1. Comparing them with the measurements, we observe a very good agreement on the spectral position and lineshape of the resonances. Importantly, the theoretical results reproduce the behavior observed in the experiment, namely the change from a size-dependent response when the nanorods are placed on silica, to a largely size-independent response when placed on the gold film. Incidentally, the theoretical predictions display slightly broader resonances than those observed in the measurements. This difference could be attributed to the larger material losses in the structures used to tabulate the dielectric function that we employ in the calculations, ⁵⁴ as compared to the expectedly more crystalline nanorods used in this experiment.

In order to verify that the behavior observed in Figure 1 is not particular to the analyzed nanorods, we measure single-particle scattering spectra for over 200 gold nanorods on each substrate (silica and gold film), with different widths and aspect ratios. The results are displayed in Figure 2. In particular, panels (a) and (b) show the scattering spectra of the individual nanorods placed on the silica and gold substrates, respectively. The results are organized based on the dimensions of the nanorods as indicated by the labels and the background color. We measure nanorods with $w = 40 \,\mathrm{nm}$ and A = 1.7, 2.2, 3.7 (which correspond to $L = 68, 88, 148 \,\mathrm{nm}$) as well as $w = 25 \,\mathrm{nm}$ and A = 2.3, 2.8, 3.6 (which correspond to $L = 58, 70, 90 \,\mathrm{nm}$), according to the specification for the colloidal solution. Examining the results of Figure 2(a), we observe a clear jump on the average peak energy when the nominal size of the gold nanorods is changed. The small fluctuation within the same type of nanorods is a consequence of the size distribution in the colloidal solution. 55

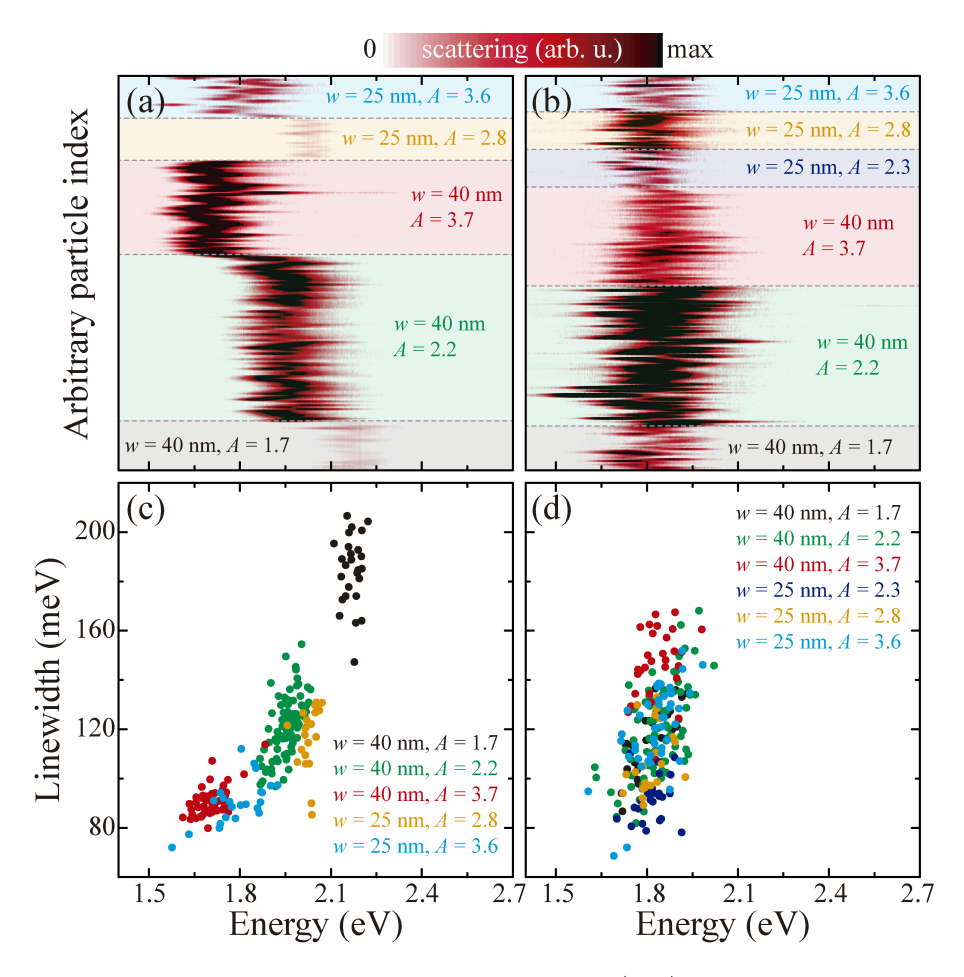


Figure 2: Characterization of the scattering spectra. (a,b) Measured single-particle scattering spectra for a large collection of different nanorods placed on the silica (a) and gold (b) substrates. The background color and labels indicate the nanorod dimensions. (c,d) Linewidths of the different spectra of panels (a) and (b) plotted as a function of the energy of the plasmon resonance. Again, the nanorod dimensions are indicated by the color of the symbol.

In contrast, as shown in Figure 2(b), when the nanorods are placed on the gold film, their resonance energy is only weakly dependent on the size and aspect ratio of the nanoparticles. Notice that all of them fall approximately within a 0.3 eV window around the same energy. Furthermore, in this case, the scattering intensity does not scale with particle size; there instead appears to be an optimal particle size that couples light into and out of the system more efficiently. Even though the average resonance energy does not change appreciably with the significant change in the aspect ratio (from 1.7 to 3.7) of the gold nanorods, there is an appreciable fluctuation from particle to particle. This effect can be attributed to the sensitivity of the response to variations in the geometry of the particle-film interface, as well as changes in the distribution of surface ligands and the chemical composition of the environment.

We further analyze the scattering behavior of the nanorods by extracting the resonance energy and linewidths from the measured data, through the fitting of a Lorentzian function to the different experimental spectra. The corresponding results are summarized in Figures 2(c) and (d). Clearly, for nanorods on the silica substrate, the linewidth increases with resonance energy. We attribute this behavior to the larger overlap of the plasmon resonance with the interband transitions of gold, which is expected to increase the nonradiative losses, thus resulting in a broader lineshape. 1,56,57 However, nanorods placed on gold show a weak relationship between linewidth and aspect ratio, with larger sizes resulting in slightly larger linewidth, as shown in Figure 2(d). It is worth noting that this relationship is the opposite of what we observe for the same nanorods placed on silica. For example, considering the nominal width of 40 nm, gold nanorods with aspect ratio of 3.7 display the narrowest linewidths when placed on silica, but the broadest linewidth when sitting on the gold film, as can be seen by comparing the data plotted in Figures 2(c) and (d). This is consistent with the fact that the radiative losses increase with nanorod volume, ¹⁷ while the nonradiative ones, which are associated with the material losses of the system, and therefore dependent on the dielectric function, stay constant due to the fixed plasmon energy.

In order to understand the origin of the difference in the response of the nanorods when placed on the silica and gold substrates, we calculate the induced charge and the radiation pattern associated with their plasmon resonance. In particular, we focus on a nanorod with $w = 40 \,\mathrm{nm}$ and A = 3.7, due to the large resonance energy shift when changing from silica to gold substrates, as shown in Figure 3(a) by the green and red curves, respectively. The corresponding induced surface charge maps are plotted in the upper panels of Figure 3(b). The results for the nanorod placed on silica (left panel) confirm the longitudinal dipolar nature of the resonance, and therefore explain the observed correlation between aspect ratio and resonance position. The associated radiation pattern confirms this result. It corresponds to a dipole oscillating parallel to the substrate with a secondary lobe structure caused by the actual shape of the nanorod facet, which breaks the symmetry of the emission pattern. As expected, the majority of the radiation is emitted into the silica substrate.⁵⁸

On the other hand, for the nanorod placed on gold (right panel), we observe a completely different charge map. In this case, we find that the plasmon response is associated with a transfer of charge between the nanorod and the film, in which the entire nanorod is positively or negatively charged, with the film having the exact opposite charge. This means that the scattering response of the nanorods placed on the gold film is dominated by a charge transfer mode. The radiation pattern corresponding to this mode is shown in the lower right panel of Figure 3(b). In this case, based on the induced charge map, we expect a dipole oscillating perpendicular to the substrate, which consequently produces a doughnut-shaped radiation pattern. This is confirmed by the calculations, which also show a secondary lobe structure caused, again, by the faceting of the nanorod. Both radiation patterns are in good agreement with the experimental dark-field images shown as insets in the lower panels. It is worth noting, that these results discard the possibility of the observed behavior being caused by the transversal mode of the nanorods.

So far, we have assumed that, when placed on the gold film, the nanorods are in conductive contact with the metallic surface. However, we know that, due to the chemical synthesis

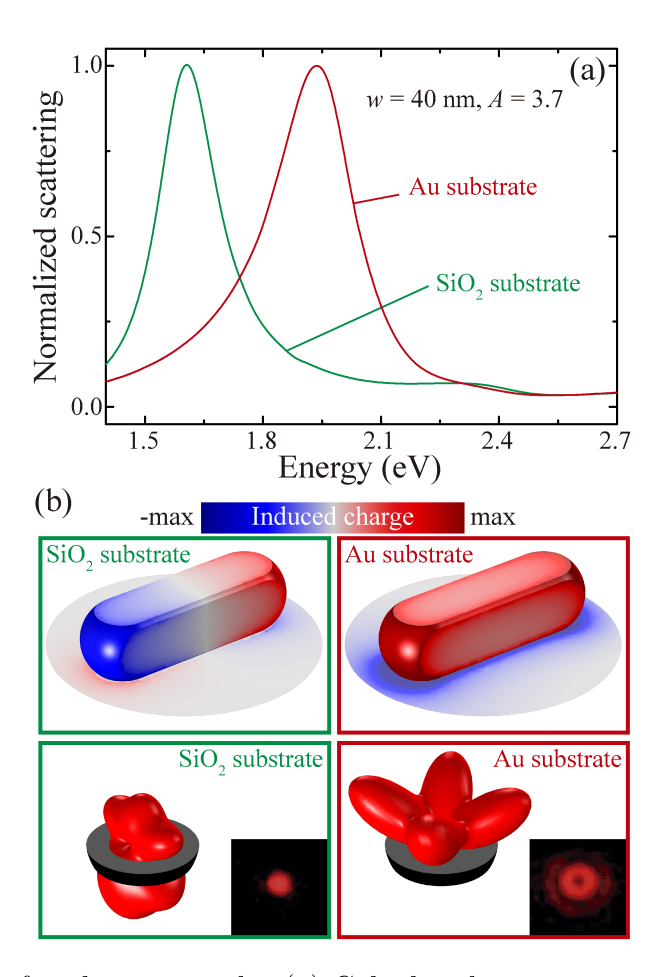


Figure 3: Charge transfer plasmon mode. (a) Calculated scattering spectra for a nanorod of width $w=40\,\mathrm{nm}$ and aspect ratio A=3.7 placed on the silica (green curve) and gold (red curve) substrates. (b) Induced surface charge maps (upper panels) and radiation pattern (lower panels) calculated at the resonance peaks of panel (a). The left and right columns display the results for silica and gold substrates, respectively. The insets in the lower panels show the experimental dark-field images.

process, the gold nanorods are partially covered by surface ligands (cetyltrimethylammonium bromide, CTAB) when they are suspended in solution, which, during the deposition process, are expected to spread across the substrate, leaving the nanorods in direct contact with it. In order to understand the role that the surface ligands can play in the optical response of the system, we repeat the calculations of the scattering response of a nanorod deposited on the gold substrate assuming, in this case, a dielectric spacer located between the nanorod and the substrate³⁰ (see Figure S2 in the Supporting Information for a detailed description of our simulation geometry). The results of this calculation are shown in Figure 4. More specifically, in panels (a) and (c), we analyze the scattering spectra of nanorods with A = 1.7 and 3.7, respectively, and fixed $w = 40 \, \text{nm}$. The solid curves display the theoretical calculations performed assuming that the nanorods are either in direct contact with the substrate (red curve), or separated from it by a 1.5 nm-thick spacer with dielectric function $\varepsilon = 2$ (green curve), while the black dots represent single-particle measurements for two nanorods of nominally the same dimensions as those modeled. Clearly, in the absence of conductive contact, the scattering spectrum displays several peaks that correspond to cavity plasmons confined to the dielectric spacer, ⁵⁹ as shown in Figure S3 of the Supporting Information. The presence of these peaks and the broader lineshape of the spectrum when compared with the corresponding one for the direct contact configuration are in sharp contrast with the experimental results. It is important to remark that none of the hundreds of single-particle measurements we have performed display any extra peak. One may argue that, due to its cavity nature, these resonances may not be visible in the experiment due to the surface roughness of the metallic film. In order to discard that possibility, we have performed a careful analysis of the topography of our metallic film, together with simulations of the scattering spectra of the system considering different types of defects in the dielectric spacer. The corresponding results, which are shown in Figures S4, S5, and S6 of the Supporting Information, show that, in all cases, several peaks are always present in the scattering spectrum when the nanorods are separated from the film by a dielectric spacer.

Interestingly, by adding a finite conductivity σ to the dielectric function of the spacer, which then becomes $\varepsilon = 2 + i\sigma/(\varepsilon_0\omega)$, it is possible to recover the results obtained for the case of the nanorod being in direct contact with the substrate. This is shown in panels (b) and (d), where we plot the scattering spectra of the nanorods calculated for different values of σ in the range $10^3 - 10^7 \,\Omega^{-1} \mathrm{m}^{-1}$, as indicated by the legend (for reference, the static conductivity of gold is $\sim 4 \times 10^7 \,\Omega^{-1} \mathrm{m}^{-1}$). Examining these results, we observe that, as the conductivity increases, the multiple peaks in the spectrum disappear and a single resonance, located at the frequency of the charge transfer plasmon, emerges. Interestingly, this transition seems to occur for values of the conductivity below $10^5 \,\Omega^{-1} \mathrm{m}^{-1}$. Beyond that value, the increase of the conductivity does not alter the spectral position of the resonance, although it makes the resonance become stronger and narrower, which is consistent with the reduced dissipation associated with an increase of the conductivity.

It is worth noting that, when comparing the spectra obtained for the nanorods sitting on the dielectric substrate with those calculated for the nanorods separated from the metallic film by a 1.5 nm-thick dielectric spacer, we observe a redshift of the scattering spectrum for the nanorod with A = 1.7, and a blueshift for the one with A = 3.7 (see Figure S7 of the Supporting Information). We attribute this behavior to the differences in the coupling between the longitudinal and transversal modes of the nanorods and the metallic film, which play an important role when the nanostructures have an aspect ratio different from 1.

The results analyzed in Figure 4 support the hypothesis that the behavior we observe in the experiment arises from the conductive coupling between the nanorod and the gold film. The experimental and theoretical results strongly suggest that the interface between the gold nanorods and the gold film is conductive, and the resonance can be described as a charge transfer plasmon. This is compatible with a low CTAB coverage on the surface of the nanorods, which we have verified by repeating the measurements shown in Figure 2 for nanorods that are prepared using a procedure that is expected to remove a larger fraction of surface ligands. As shown in Figure S8 of the Supporting Information, the new results

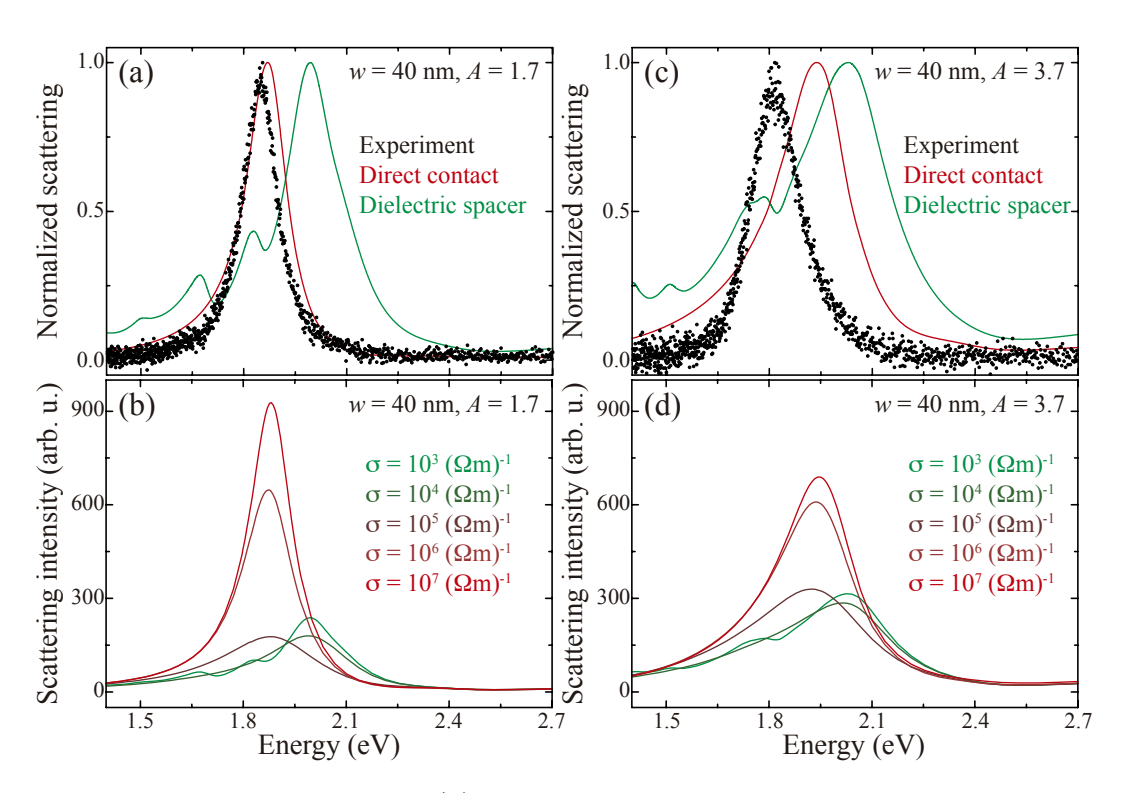


Figure 4: Effect of surface ligands. (a) Normalized scattering spectra of a nanorod of $w=40\,\mathrm{nm}$ and A=1.7 placed on the gold substrate. The solid curves show the theoretical predictions assuming the nanorod is in direct contact with the substrate (red curve), or is separated from it by a 1.5 nm-thick dielectric spacer with dielectric function $\varepsilon=2$ (green curve), while the black dots correspond to the experimental single-particle measurements. (b) Comparison of the scattering spectra of the nanorod of panel (a) for different values of conductivity of the dielectric spacer, as indicated by the legend. (c,d) Same as (a,b), but for a nanorod of $w=40\,\mathrm{nm}$ and A=3.7.

are similar to those of Figure 2, which supports our claim. Indeed, a recent work has shown that the CTAB coverage on the surface of nanorods is not uniform. 60 This, together with the surface roughness of the metallic film (see Figure S4), can enable sufficient contact points between the nanorod and the film. Furthermore, theoretical calculations have shown that, for gaps of $\sim 0.4 \,\mathrm{nm}$, the conductivity arising from tunneling processes can be larger than $10^5 \,\Omega^{-1}\mathrm{m}^{-1}$ for moderate electric fields. 61

The questions that are now posed are why there is a conductivity threshold for the charge transfer mode, and why its frequency is so weakly dependent on the dimensions of the nanorod. In order to answer these questions, we use a simple analytical model similar to that presented by Pérez-González et al. 45 to explain the behavior of charge transfer plasmons in plasmonic nanoparticle dimers bridged by conductive junctions. We first assume that the combined nanorod and substrate system acts as a capacitor with a conductive junction connecting the two elements. When illuminated, the amount of charge flowing between the particle and the film, associated with the excitation of the charge transfer plasmon mode, must be such that it cancels out the field induced between the nanorod and the film. Therefore, in a first approximation, and ignoring any inhomogeneity of the field within the facet of the nanoparticles, this charge can be written as $Q = CdE_{ind}$, where E_{ind} is the induced field, C is the capacitance of the system, and d the distance between the two elements. The product Cd defines an effective capacitance area $A_c = Cd/\varepsilon_0$, which depends exclusively on the geometry of the nanorod-film junction. For instance, if, instead of a nanorod, an extended planar surface is considered, A_c corresponds to the surface area. On the other hand, the current flowing between the nanorod and the film can be approximated as $I = \sigma A_j E_{ind}$, where σ is the conductivity of the junction, and A_j is the junction area, which, in our case, is equal to the facet area. Then, the frequency of the charge transfer plasmon. $\omega_{\rm CTP}$, can be obtained from the ratio I/Q. By doing so, we can write $\sigma \propto \omega_{\rm CTP} A_c/A_j$. This equation states that, for a given system, there is a minimum conductivity necessary to sustain the charge transfer plasmon, in accordance with the results of Figures 4(b) and (d). Furthermore, in the limit of large conductivity (i.e., beyond the conductivity threshold), the frequency of the plasmon is expected to scale as A_j/A_c . Then, ignoring the effect of the hemispherical ends of the nanorods, A_c is proportional to the surface area of the nanorod, and therefore to w. This makes the ratio between the junction and capacitance areas independent of the length of the nanorod (since both of them are proportional to it), thus depending only on the ratio between the facet and the nanorod widths, i.e., $A_j/A_c \approx w_f/w$. Accordingly, we expect the frequency of the charge transfer plasmon to scale with w_f/w , which can be understood as the "squareness" of the nanorod, as shown in the inset of Figure 5.

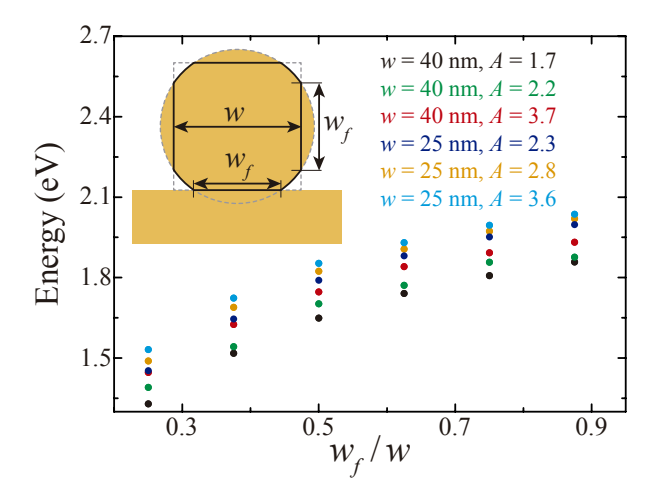


Figure 5: Effect of particle shape on the charge transfer plasmon resonance. Energy of the plasmon resonance as a function of the "squareness" of the nanorods, calculated for multiple nanorods of varied width w and aspect ratio A, as indicated by dot color and the legend. Squareness is defined as the ratio between the width of the facet w_f and width of the nanorod w, as depicted in the inset.

To test the predictions of this model, we calculate the scattering spectra of nanorods placed in direct contact with a gold substrate, and with the same widths and aspect ratios as those analyzed in Figure 2, but varying their w_f/w ratio. We plot the energy of the resulting scattering peaks in Figure 5 as a function of w_f/w , using dots of different colors for the different nanorods, as indicated by the legend. Examining these results, we observe that, as w_f/w increases and approaches 1 (i.e., a square transversal cross section), the peak energies are blue shifted and tend to an asymptote, as predicted by our model. Furthermore,

we find that, for each value of w_f/w , the resonance energies of all of the nanorods investigated fall within a $\lesssim 0.3\,\mathrm{eV}$ window, in good agreement with the experiments (see Figure 2), for which we expect a uniform value of w_f/w determined by the synthesis of the nanorods. This confirms that the weak dependence of the scattering spectrum of the gold nanorods deposited on the gold film arises from the charge transfer nature of the resonance. We attribute the 0.3 eV variation to the effect played by the hemispherical ends of the nanorods, which is expected to change with their dimensions. Interestingly, the scattering spectra of nanorods placed on silica are almost independent of the value w_f/w as shown in Figure S9 of the Supporting Information, which is consistent with the dipolar character of the dominant resonance of the scattering spectra of these structures.

In summary, we have presented a detailed experimental and theoretical study of the optical response of gold nanorods placed on both silica and gold substrates. We have found that, for nanorods placed on silica, the response is dominated by a dipolar surface plasmon whose characteristics are very dependent on the size and aspect ratio of the nanorod. On the contrary, when the same nanorods are placed on a gold substrate, the scattering spectrum displays a strong charge transfer plasmon resonance, for which charge flows between the particle and the substrate. This mode, in contrast to the typical dipolar resonance, is always located around the same energy, regardless of the width and aspect ratio of the nanorod. Using rigorous solutions of Maxwell's equations, as well as a simple analytical model, we have shown that the properties of this mode are dictated by the characteristics of the particle-film junction. The results presented here provide new insights into the interaction of metallic nanoparticles with metallic substrates, which could be exploited to design plasmonic systems that are more robust against variations in the nanoparticle geometry.

Acknowledgement

The experimental component of this research has been supported by the U.S. Air Force Of-

fice of Scientific Research, Grant No. FA9550-15-1-0305, while the theoretical part has been partially supported by the U.S. National Science Foundation (Grant ECCS-1710697). In the final phase of the work, BK has been supported by the U.S. National Science Foundation (Grant CHE-1651478). PG thanks financial support from the UNM NSMS program through the Whitten Family Fellowship. We would like to thank the UNM Center for Advanced Research Computing, supported in part by the U.S. National Science Foundation, for providing the high performance computing resources used in this work.

Supporting Information Available

We provide: (i) detailed information about the experimental setup and the numerical calculations, (ii) an analysis of the scattering spectrum of gold nanorods separated from the metallic substrate by a dielectric spacer, (iii) a careful characterization of the topography of the metallic film, and (iv) an additional analysis of the dependence of the nanorods scattering spectra on the facet size.

References

- (1) Maier, S. A. Plasmonics: Fundamentals and Applications; Springer: New York, 2007.
- (2) Schuller, J. A.; Barnard, E. S.; Cai, W.; Jun, Y. C.; White, J. S.; Brongersma, M. L. Plasmonics for extreme light concentration and manipulation. *Nat. Mater.* 2010, 9, 193–204.
- (3) Álvarez-Puebla, R. A.; Liz-Marzán, L. M.; García de Abajo, F. J. Light concentration at the nanometer scale. *J. Phys. Chem. Lett.* **2010**, *1*, 2428–2434.
- (4) Atwater, H. A.; Polman, A. Plasmonics for improved photovoltaic devices. *Nat. Mater.* 2010, 9, 205–213.

- (5) Lee, J.; Mubeen, S.; Ji, X.; Stucky, G. D.; Moskovits, M. Plasmonic photoanodes for solar water splitting with visible light. *Nano Lett.* **2012**, *12*, 5014–5019.
- (6) Brongersma, M. L.; Halas, N. J.; Nordlander, P. Plasmon-induced hot carrier science and technology. *Nat. Nanotechnol.* **2015**, *10*, 25–34.
- (7) Tesema, T. E.; Kafle, B.; Tadesse, M. G.; Habteyes, T. G. Plasmon-Enhanced Resonant Excitation and Demethylation of Methylene Blue. J. Phys. Chem. C 2017, 121, 7421– 7428.
- (8) Xu, H.; Bjerneld, E. J.; Käll, M.; Börjesson, L. Spectroscopy of single hemoglobin molecules by surface enhanced Raman scattering. Phys. Rev. Lett. 1999, 83, 4357– 4360.
- (9) Moskovits, M. Surface-enhanced Raman spectroscopy: a brief retrospective. *J. Raman Spectrosc.* **2005**, *36*, 485–496.
- (10) Chen, X.; Cirací, C.; Smith, D. R.; Oh, S.-H. Nanogap-enhanced infrared spectroscopy with template-stripped wafer-scale arrays of buried plasmonic cavities. *Nano Lett.* 2015, 15, 107–113.
- (11) Ding, S.-Y.; You, E.-M.; Tian, Z.-Q.; Moskovits, M. Electromagnetic theories of surface-enhanced Raman spectroscopy. *Chem. Soc. Rev.* **2017**, *46*, 4042–4076.
- (12) Myroshnychenko, V.; Carbó-Argibay, E.; Pastoriza-Santos, I.; Pérez-Juste, J.; Liz-Marzán, L. M.; García de Abajo, F. J. Modelling the optical response of highly faceted metal nanoparticles with a fully 3D boundary element method. Adv. Mater. 2008, 20, 4288–4293.
- (13) Knight, M. W.; Wu, Y.; Lassiter, J. B.; Nordlander, P.; Halas, N. J. Substrates Matter: Influence of an Adjacent Dielectric on an Individual Plasmonic Nanoparticle. *Nano Lett.* 2009, 9, 2188–2192.

- (14) Aravind, P. K.; Metiu, H. Use of a perfectly conducting sphere to excite the plasmon of a flat surface. 1. Calculation of the local field with applications to surface-enhanced spectroscopy. J. Phys. Chem. 1982, 86, 5076–5084.
- (15) Lévêque, G.; Martin, O. J. F. Optical interactions in a plasmonic particle coupled to a metallic film. *Opt. Express* **2006**, *14*, 9971–9981.
- (16) Mock, J. J.; Hill, R. T.; Degiron, A.; Zauscher, S.; Chilkoti, A.; Smith, D. R. Distance-Dependent Plasmon Resonant Coupling between a Gold Nanoparticle and Gold Film. Nano Lett. 2008, 8, 2245–2252.
- (17) Sobhani, A.; Manjavacas, A.; Cao, Y.; McClain, M. J.; García de Abajo, F. J.; Nordlander, P.; Halas, N. J. Pronounced Linewidth Narrowing of an Aluminum Nanoparticle Plasmon Resonance by Interaction with an Aluminum Metallic Film. *Nano Lett.* 2015, 15, 6946–6951.
- (18) Esteban, R.; Aguirregabiria, G.; Borisov, A. G.; Wang, Y. M.; Nordlander, P.; Bryant, G. W.; Aizpurua, J. The Morphology of Narrow Gaps Modifies the Plasmonic Response. *ACS Photonics* **2015**, *2*, 295–305.
- (19) Ciracì, C.; Hill, R. T.; Mock, J. J.; Urzhumov, Y.; Fernández-Domínguez, A. I.; Maier, S. A.; Pendry, J. B.; Chilkoti, A.; Smith, D. R. Probing the ultimate limits of plasmonic enhancement. Science 2012, 337, 1072–1074.
- (20) Lassiter, J. B.; McGuire, F.; Mock, J. J.; Ciracì, C.; Hill, R. T.; Wiley, B. J.; Chilkoti, A.; Smith, D. R. Plasmonic Waveguide Modes of Film-Coupled Metallic Nanocubes. *Nano Lett.* 2013, 13, 5866–5872.
- (21) Tserkezis, C.; Esteban, R.; Sigle, D. O.; Mertens, J.; Herrmann, L. O.; Baumberg, J. J.; Aizpurua, J. Hybridization of plasmonic antenna and cavity modes: Extreme optics of nanoparticle-on-mirror nanogaps. *Phys. Rev. A* 2015, *92*, 053811.

- (22) Huang, S.; Ming, T.; Lin, Y.; Ling, X.; Ruan, Q.; Palacios, T.; Wang, J.; Dresselhaus, M.; Kong, J. Ultrasmall Mode Volumes in Plasmonic Cavities of Nanoparticle-on-Mirror Structures. *Small* **2016**, *12*, 5190–5199.
- (23) Chikkaraddy, R.; Zheng, X.; Benz, F.; Brooks, L. J.; de Nijs, B.; Carnegie, C.; Kleemann, M.-E.; Mertens, J.; Bowman, R. W.; Vandenbosch, G. A. E.; Moshchalkov, V. V.; Baumberg, J. J. How Ultranarrow Gap Symmetries Control Plasmonic Nanocavity Modes: From Cubes to Spheres in the Nanoparticle-on-Mirror. ACS Photonics 2017, 4, 469–475.
- (24) Mertens, J.; Eiden, A. L.; Sigle, D. O.; Huang, F.; Lombardo, A.; Sun, Z.; Sundaram, R. S.; Colli, A.; Tserkezis, C.; Aizpurua, J.; Milana, S.; Ferrari, A. C.; Baumberg, J. J. Controlling Subnanometer Gaps in Plasmonic Dimers Using Graphene. *Nano Lett.* **2013**, *13*, 5033–5038.
- (25) Hu, M.; Ghoshal, A.; Marquez, M.; Kik, P. G. Single Particle Spectroscopy Study of Metal-Film-Induced Tuning of Silver Nanoparticle Plasmon Resonances. J. Phys. Chem. C 2010, 114, 7509–7514.
- (26) Lumdee, C.; Toroghi, S.; Kik, P. G. Post-fabrication Voltage Controlled Resonance Tuning of Nanoscale Plasmonic Antennas. *ACS Nano* **2012**, *6*, 6301–6307.
- (27) Moreau, A.; Ciraci, C.; Mock, J. J.; Hill, R. T.; Wang, Q.; Wiley, B. J.; Chilkoti, A.; Smith, D. R. Controlled-reflectance surfaces with film-coupled colloidal nanoantennas. Nature 2012, 492, 86–89.
- (28) Mock, J. J.; Hill, R. T.; Tsai, Y.-J.; Chilkoti, A.; Smith, D. R. Probing Dynamically Tunable Localized Surface Plasmon Resonances of Film-Coupled Nanoparticles by Evanescent Wave Excitation. *Nano Lett.* **2012**, *12*, 1757–1764.
- (29) Kafle, B.; Poveda, M.; Habteyes, T. G. Surface Ligand-Mediated Plasmon-Driven Photochemical Reactions. *J. Phys. Chem. Lett.* **2017**, *8*, 890–894.

- (30) Huh, J.-H.; Lee, J.; Lee, S. Comparative Study of Plasmonic Resonances between the Roundest and Randomly Faceted Au Nanoparticles-on-Mirror Cavities. *ACS Photonics* **2018**, *5*, 413–421.
- (31) Taylor, R. W.; Benz, F.; Sigle, D. O.; Bowman, R. W.; Bao, P.; Roth, J. S.; Heath, G. R.; Evans, S. D.; Baumberg, J. J. Watching individual molecules flex within lipid membranes using SERS. *Sci. Rep.* **2014**, *4*, 5940.
- (32) Benz, F.; Tserkezis, C.; Herrmann, L. O.; de Nijs, B.; Sanders, A.; Sigle, D. O.; Pukenas, L.; Evans, S. D.; Aizpurua, J.; Baumberg, J. J. Nanooptics of Molecular-Shunted Plasmonic Nanojunctions. *Nano Lett.* 2015, 15, 669–674.
- (33) Liu, P.; Chulhai, D. V.; Jensen, L. Single-Molecule Imaging Using Atomistic Near-Field Tip-Enhanced Raman Spectroscopy. ACS Nano 2017, 11, 5094–5102.
- (34) Benz, F.; Schmidt, M. K.; Dreismann, A.; Chikkaraddy, R.; Zhang, Y.; Demetriadou, A.; Carnegie, C.; Ohadi, H.; Nijs, B. d.; Esteban, R.; Aizpurua, J.; Baumberg, J. J. Single-molecule optomechanics in "picocavities". *Science* **2016**, *354*, 726–729.
- (35) Kleemann, M.-E.; Chikkaraddy, R.; Alexeev, E. M.; Kos, D.; Carnegie, C.; Deacon, W.; Pury, A. C.; Große, C.; Nijs, B.; Mertens, J.; Tartakovskii, A. I.; Baumberg, J. J. Strong-coupling of WSe₂ in ultra-compact plasmonic nanocavities at room temperature. *Nat. Commun.* **2017**, *8*, 1296.
- (36) Akselrod, G. M.; Argyropoulos, C.; Hoang, T. B.; Ciracì, C.; Fang, C.; Huang, J.; Smith, D. R.; Mikkelsen, M. H. Probing the mechanisms of large Purcell enhancement in plasmonic nanoantennas. *Nat. Photonics* 2014, 8, 835–840.
- (37) Hoang, T. B.; Akselrod, G. M.; Argyropoulos, C.; Huang, J.; Smith, D. R.; Mikkelsen, M. H. Ultrafast spontaneous emission source using plasmonic nanoantennas.

 Nat. Commun. 2015, 6, 7788.

- (38) Huang, J.; Akselrod, G. M.; Ming, T.; Kong, J.; Mikkelsen, M. H. Tailored Emission Spectrum of 2D Semiconductors Using Plasmonic Nanocavities. *ACS Photonics* **2018**, 5, 552–558.
- (39) Stewart, J. W.; Akselrod, G. M.; Smith, D. R.; Mikkelsen, M. H. Toward Multispectral Imaging with Colloidal Metasurface Pixels. *Adv. Mater.* **2017**, *29*, 1602971.
- (40) Martin, J. E.; Wilcoxon, J. P.; Odinek, J.; Provencio, P. Control of the Interparticle Spacing in Gold Nanoparticle Superlattices. *J. Phys. Chem. B* **2000**, *104*, 9475–9486.
- (41) Sau, T. K.; Murphy, C. J. Self-Assembly Patterns Formed upon Solvent Evaporation of Aqueous Cetyltrimethylammonium Bromide-Coated Gold Nanoparticles of Various Shapes. *Langmuir* 2005, 21, 2923–2929.
- (42) Gómez-Graña, S.; Hubert, F.; Testard, F.; Guerrero-Martínnez, A.; Grillo, I.; Liz-Marzán, L. M.; Spalla, O. Surfactant (Bi)Layers on Gold Nanorods. Langmuir 2012, 28, 1453–1459.
- (43) Chen, X.; Moore, J. E.; Zekarias, M.; Jensen, L. Atomistic electrodynamics simulations of bare and ligand-coated nanoparticles in the quantum size regime. *Nat. Commun.* **2015**, *6*, 8921.
- (44) Hore, M. J. A.; Ye, X.; Ford, J.; Gao, Y.; Fei, J.; Wu, Q.; Rowan, S. J.; Composto, R. J.; Murray, C. B.; Hammouda, B. Probing the Structure, Composition, and Spatial Distribution of Ligands on Gold Nanorods. *Nano Lett.* 2015, 15, 5730–5738.
- (45) Pérez-González, O.; Zabala, N.; Borisov, A. G.; Halas, N. J.; Nordlander, P.; Aizpurua, J. Optical Spectroscopy of Conductive Junctions in Plasmonic Cavities. *Nano Lett.* 2010, 10, 3090–3095.
- (46) Pérez-González, O.; Zabala, N.; Aizpurua, J. Optical characterization of charge trans-

- fer and bonding dimer plasmons in linked interparticle gaps. New J. Phys. **2011**, 13, 083013.
- (47) Pérez-González, O.; Aizpurua, J.; Zabala, N. Optical transport and sensing in plexcitonic nanocavities. *Opt. Express* **2013**, *21*, 15847–15858.
- (48) Wang, Y.; Li, Z.; Zhao, K.; Sobhani, A.; Zhu, X.; Fang, Z.; Halas, N. J. Substrate-mediated charge transfer plasmons in simple and complex nanoparticle clusters.

 Nanoscale 2013, 5, 9897–9901.
- (49) Wen, F.; Zhang, Y.; Gottheim, S.; King, N. S.; Zhang, Y.; Nordlander, P.; Halas, N. J. Charge Transfer Plasmons: Optical Frequency Conductances and Tunable Infrared Resonances. ACS Nano 2015, 9, 6428–6435.
- (50) Song, P.; Nordlander, P.; Gao, S. Quantum mechanical study of the coupling of plasmon excitations to atomic-scale electron transport. *J. Chem. Phys.* **2011**, *134*, 074701.
- (51) Tan, S. F.; Wu, L.; Yang, J. K.; Bai, P.; Bosman, M.; Nijhuis, C. A. Quantum plasmon resonances controlled by molecular tunnel junctions. *Science* **2014**, *343*, 1496–1499.
- (52) Kulkarni, V.; Manjavacas, A. Quantum Effects in Charge Transfer Plasmons. *ACS Photonics* **2015**, *2*, 987–992.
- (53) Knebl, D.; Hörl, A.; Trügler, A.; Kern, J.; Krenn, J. R.; Puschnig, P.; Hohenester, U. Gap plasmonics of silver nanocube dimers. *Phys. Rev. B* **2016**, *93*, 081405.
- (54) Johnson, P. B.; Christy, R. W. Optical constants of the noble metals. *Phys. Rev. B* 1972, 6, 4370–4379.
- (55) Habteyes, T. G. Direct Near-Field Observation of Orientation-Dependent Optical Response of Gold Nanorods. J. Phys. Chem. C 2014, 118, 9119–9127.

- (56) Sönnichsen, C.; Franzl, T.; Wilk, T.; von Plessen, G.; Feldmann, J.; Wilson, O.; Mulvaney, P. Drastic Reduction of Plasmon Damping in Gold Nanorods. *Phys. Rev. Lett.* 2002, 88, 077402.
- (57) Novo, C.; Gomez, D.; Perez-Juste, J.; Zhang, Z.; Petrova, H.; Reismann, M.; Mulvaney, P.; Hartland, G. V. Contributions from radiation damping and surface scattering to the linewidth of the longitudinal plasmon band of gold nanorods: a single particle study. *Phys. Chem. Chem. Phys.* **2006**, *8*, 3540–3546.
- (58) Novotny, L.; Hecht, B. *Principles of Nano-Optics*; Cambridge University Press: New York, 2006.
- (59) Jung, J.; Söndergaard, T.; Bozhevolnyi, S. I. Gap plasmon-polariton nanoresonators: Scattering enhancement and launching of surface plasmon polaritons. *Phys. Rev. B* **2009**, *79*, 035401.
- (60) González-Rubio, G.; Díaz-Nuñez, P.; Rivera, A.; Prada, A.; Tardajos, G.; González-Izquierdo, J.; Bañares, L.; Llombart, P.; Macdowell, L. G.; Palafox, M. A.; Liz-Marzán, L. M.; Peñ-Rodríguez, O.; Guerrero-Martínez, A. Femtosecond laser reshaping yields gold nanorods with ultranarrow surface plasmon resonances. Science 2017, 358, 640-644.
- (61) Wu, L.; Duan, H.; Bai, P.; Bosman, M.; Yang, J. K. W.; Li, E. Fowler-Nordheim Tunneling Induced Charge Transfer Plasmons between Nearly Touching Nanoparticles. ACS Nano 2013, 7, 707–716.

Graphical TOC Entry

